Determination of the beam asymmetry Σ in η- and η'-photoproduction using Bayesian statistics

Jakob Michael Krause

Masterarbeit in Physik
angefertigt im Helmholtz-Institut für Strahlen- und Kernphysik

vorgelegt der
Mathematisch-Naturwissenschaftlichen Fakultät
der
Rheinischen Friedrich-Wilhelms-Universität
Bonn

Sep 2022

I hereby declare that this thesis was formulated by myself and that no sources or tools other than those cited were used.

Bonn, ...
Date Signature

1. Gutachterin: Jun. Prof. Dr. Annika Thiel
2. Gutachter: Prof. Dr. Jochen Dingfelder

Contents

CHAPTER 1

Introduction

The *Standard Model of Particle Physics* (SM) is the most successful model aiming to describe the particles and forces of the universe. It distinguishes between *fermions* and *bosons*. While all matter consists of fermions, bosons are particles that mediate the fundamental interactions.

Matter consists of (anti-)quarks and (anti-)leptons with three generations of each. Table 1.1 shows all elementary fermions including some of their most important properties. Only the first and lightest generation consists of stable particles, i.e. the up and down quark as well as the electron and its neutrino. All other particles are heavier and not stable, they will thus decay fast via the strong, electromagnetic or weak interaction.

There are in fact four interactions described by the SM: strong, electromagnetic, weak and gravitational interaction [1], where gravitation is mentioned here for the sake of completeness; on the mass scale of elementary particles gravitation is negligible. Strong and weak interaction are restricted to a finite range of the order of the nucleon radius, whereas electromagnetic interaction and gravitation have infinite range. Each interaction has its own coupling (charge). The strong interaction is mediated by gluons and couples to the color charge.

	Generation			el. charge	color charge
	1	2	3		
Quarks	u	c	t	2/3	r,g,b
	d	s	b	1/3	r,g,b
Leptons	e	μ	τ	-1	-
	ν_e	ν_μ	ν_τ	0	-

Table 1.1: Summary of the particles of the SM

Gluons and quarks carry color charge and thus interact strongly. However, an isolated quark or gluon has not been observed. Only color neutral bound systems of quarks are seen, which are called hadrons. Hadrons with integer spin are called mesons and those with half-integer spin are called baryons. Color neutrality demands mesons consist of at least one quark and one anti-quark and baryons consist of at least three quarks.

[1] they are ordered here according to their relative strength

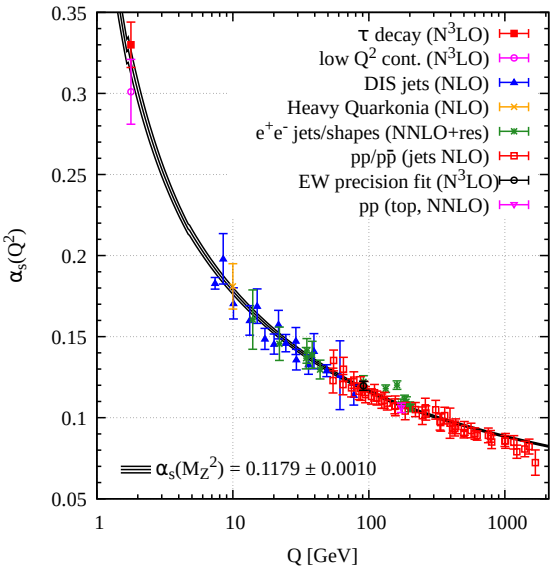

Figure 1.1: Running coupling of QCD. The colored data points represent different methods to obtain a value for α_s. For more details it may be referred to [Zyl+20].

As already mentioned, isolated quarks are not seen. This can be understood in terms of the strong coupling constant α_s. The coupling constant is a measure of the strength of the strong interaction. Because it is highly dependent on the momentum transfer in the observed strong reaction it is also called running coupling constant, which is depicted in figure 1.1.

For low (< 1 GeV) momentum transfers or large distances the coupling constant approaches infinity whereas it decreases for high ($\gg 1$ GeV) momentum transfers or short distances. These momentum ranges are referred to as *confinement* and *asymptotic freedom*, respectively; quarks are confined to remain in a bound state since if one tried to pull them apart the color field becomes so strong it will create a new quark anti-quark pair resulting in two new bound states. On the other hand, bound quarks behave quasi-free and can be described using perturbative quantum chromodynamics (pQCD) if probed at sufficiently large momentum transfers.

It is more difficult however to describe QCD at momentum scales of ≈ 1 GeV since the coupling is too strong to justify a perturbative approach. Thus explicit modeling of QCD bound states is inevitable. One possibility is to describe baryons consisting of constituent quarks which are bound in a potential. Constituent quark models assume baryons are made up of three constituent quarks with effective masses differing from the bare quark mass. The effective mass is made up mostly from a sea of quark anti-quark pairs and gluons which surround the bare (valence) quarks. The explicit form of the binding potential is determined for each model.

The Bonn model [LMP01], for example, is formulated as a relativistically covariant constituent quark model. A potential increasing linearly with the distance is employed to adequately describe confinement. The binding potential between the constituent quarks is described by an instanton-induced interaction. Baryon resonances are then states with an orbital or angular excitation of one of the quarks. Figure 1.2 shows computed nucleon, that is Isospin $I = 1/2$ resonances, of the Bonn model [LMP01] on the left side of each column. These are compared to measured resonances and their PDG rating [Zyl+20] in the middle. Uncertainties are indicated by the colored areas. The resonances are

identified by their total angular momentum and their parity $J\pi$. In addition also the total internal angular momentum along with isospin and again the total angular momentum L_{2T2J} is given. While

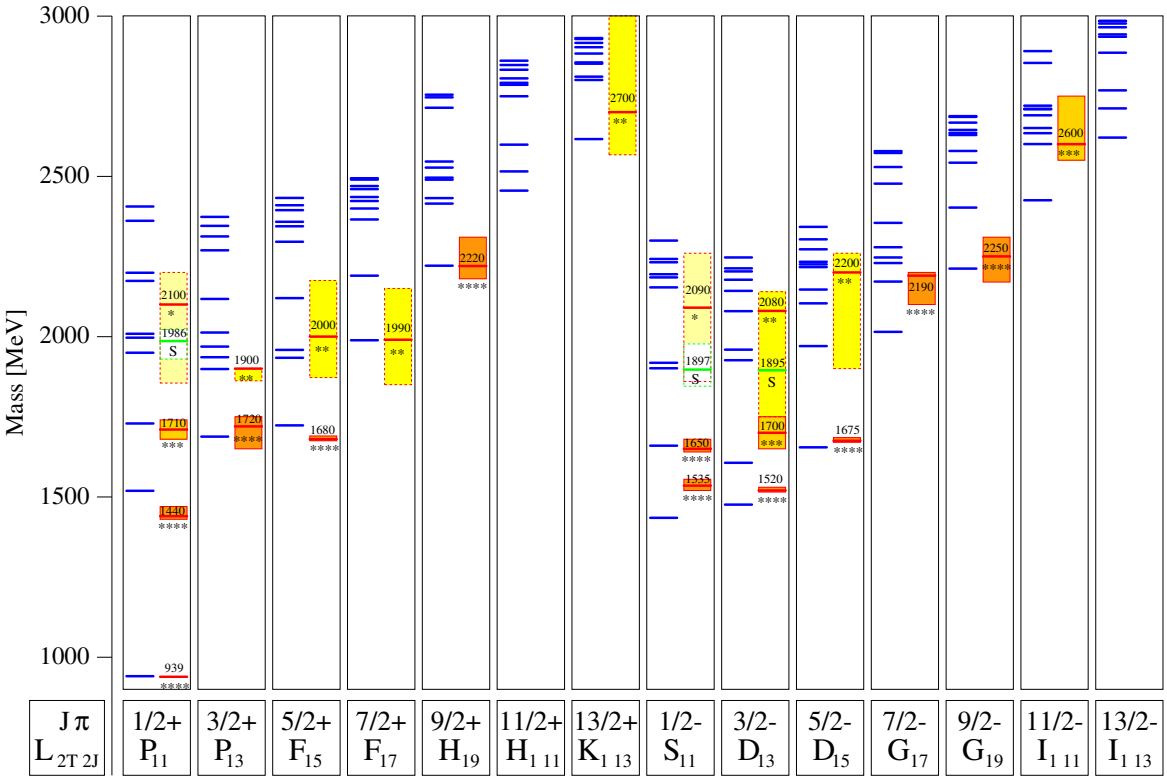

Figure 1.2: Calculated nucleon (isospin $I = 1/2$) resonances compared to measurements. Left in each column are the calculations [LMP01], the middle shows the measurements and PDG rating [Zyl+20]

generally good agreement exists for low lying resonances, especially for high masses there are much more resonances predicted than actually found. This is also known as the problem of the "missing resonances" indicating the poor understanding of QCD in the non-perturbative region. This can be due to several reasons: most of the knowledge about nucleon resonances and their properties was obtained investigating the πN channel, biasing the data for resonances coupling weakly to this channel. Furthermore, the number of excited states with definite quantum numbers is related directly to the effective number of degrees-of-freedom accessible to the underlying theory. As a consequence, the number of degrees-of-freedom should be obtainable by comparing the measured states to the predicted states. Since nucleon resonances decay dominantly hadronic, their resonances are broad and overlapping. Thus on one hand the determination of excitation spectra proves to be a challenge on its own, demanding sophisticated methods, such as partial wave analysis (PWA). On the other hand it is not yet clear how many effective degrees-of-freedom exist for the nucleon in a constituent quark model. They could for example be decreased if the nucleon were made up of a quark and a di-quark structure. In either case it should prove fruitful to investigate the photoproduction of mesons off the nucleon for different final states to access the resonances and transitions between them which are of interest. This should ultimately add to the understanding of QCD in the non-perturbative regime. [KS03]

1.1 Photoproduction of Pseudoscalar Mesons

From the scattering theory point of view, photoproduction of mesons is well understood [KS03]. Figure 1.3 shows schematically the process thereof off the proton:

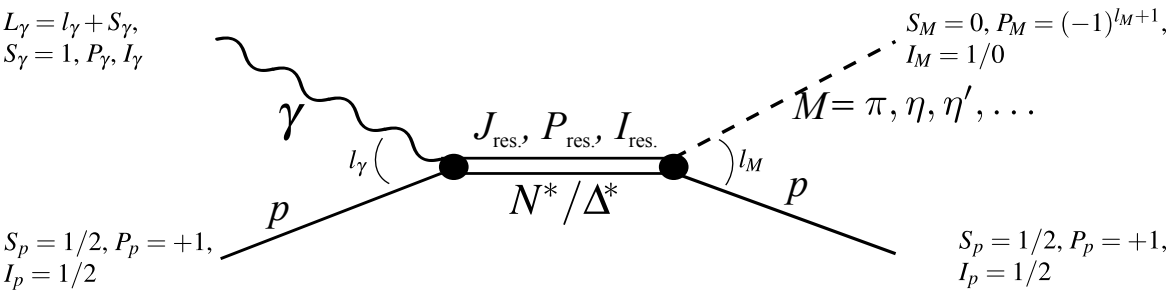

Figure 1.3: FEYNMAN diagram for the s-channel photoproduction of pseudoscalar mesons, adapted from [Afz19]

The analysis requires partial wave decomposition in both initial and final states [DT92] since the intermediate resonance has definite angular momentum, parity and isospin $J_{\text{res.}}, P_{\text{res.}}, I_{\text{res.}}$. The resonance is excited by a photon with (iso-) spin $I_\gamma, S_\gamma = 1$ and parity P_γ coupling electromagnetically to the target proton with (iso-) spin $I_p = 1/2, S_p = 1/2$ and parity P_p. The relative momentum is l_γ, such that the total momentum of the photon is $L_\gamma = l_\gamma + S_\gamma$. Subsequently the intermediate state will have the quantum numbers $J_{\text{res.}}, P_{\text{res.}}, I_{\text{res.}}$ and decay into a pseudoscalar ($S_M = 0$) meson with isospin I_M, relative orbital angular momentum l_M und Parity $P_M = (-1)^{l_M+1}$ and a proton. The following selection rules can be derived using parity and momentum conservation [KS03; Afz19]

$$J_{\text{res.}} = L_\gamma \oplus S_p = L_\gamma \oplus 1/2, \tag{1.1}$$
$$P_{\text{res.}} = P_p \cdot P_\gamma = P_\gamma, \tag{1.2}$$
$$J_{\text{res.}} = l_M \oplus S_p = l_M \oplus 1/2 \tag{1.3}$$
$$P_{\text{res.}} = P_p \cdot P_M = (-1)^{l_M+1}, \tag{1.4}$$

where the usual rules for the coupling of angular momenta [Bar+18] apply. Thus, knowledge of the photoproduction multipoles allows the identification of contributing resonances for particular mesonic final states. Table 1.2 shows relevant resonances for the lowest order of photon multipoles ($L_\gamma = 1$).

E

Table 1.2: Allowed quantum numbers for the intermediate resonance state N^*/Δ^*

1.2 Measurement of Polarization Observables

1.3 Introduction to Bayesian statistics

1.3.1 Frequentist Approach

The traditional approach to this fitting problem is a χ^2 fit. Assume there are N precise predictors $\{x_i\}$ and corresponding measurements $\{y_i\}$ with measurement errors $\{\sigma_i\}$. Additionally, the data y is expected to follow a functional $y = f(x, \boldsymbol{\theta})$ with parameter(s) $\boldsymbol{\theta}$ and predictors x. Then the test statistic

$$\chi^2 = \sum_{i=1}^{N} \left[\frac{y_i - f(x_i; \boldsymbol{\theta})}{\sigma_i^2} \right] \tag{1.5}$$

can be minimized with respect to the parameters $\boldsymbol{\theta}$ giving according estimates with error bars which are calculated using error propagation from the original data points $\{y_i\}$. The minimization can be solved analytically in the case of linear functions by solving the equation system

$$\frac{\mathrm{d}}{\mathrm{d}\boldsymbol{\theta}} \chi^2 = 0$$

and otherwise numerically. The minimization of χ^2 to get best-fit estimates for the desired parameters can be motivated if one considers the likelihood $\mathcal{L}$ that the data follow the function f. It is given by

$$\ln \mathcal{L} = -\frac{1}{2} \sum_{i=1}^{N} \left[\frac{y_i - f(x_i; \boldsymbol{\theta})}{\sigma_i} \right]^2 - \sum_{i=1}^{N} \ln \sigma_i \sqrt{2\pi}, \tag{1.6}$$

if one assumes Gaussian errors at each data point. To maximize the (log-) likelihood with respect to all parameters is then equivalent to minimizing χ^2. As a byproduct, the χ^2 fit also gives a goodness of fit estimate which is given by $\chi^2/\mathrm{NDF} \approx 1$, where NDF are the number of degrees of freedom. Significantly smaller or larger values indicate too small error estimates or a bad fit, respectively. [Bar89]

1.3.2 Bayesian approach

As an alternative

1.4 Motivation and Structure of this Thesis

bla

CHAPTER 4

Extraction of the beam asymmetries Σ_η and $\Sigma_{\eta'}$

The beam asymmetry Σ is observable when a linearly polarized photon beam and unpolarized liquid hydrogen target are employed. The polarized cross section $\frac{d\sigma}{d\Omega}_{pol}$ is not symmetric in the azimuthal angle ϕ anymore as opposed to the unpolarized cross section $\frac{d\sigma}{d\Omega}_0$. It is rather modulated by a cosine dependence which scales with the polarization observable Σ and the (linear) beam polarization p_γ, see equation (4.1) [San+11].

$$\frac{d\sigma}{d\Omega}_{pol}\left(E_\gamma, \cos\theta, \phi\right) = \frac{d\sigma}{d\Omega}_0\left(E_\gamma, \cos\theta\right) \cdot \left[1 - p_\gamma \Sigma\left(E_\gamma, \cos\theta\right) \cos\left(2\varphi\right)\right] \tag{4.1}$$

Since the incident photon beam is polarized, photon momentum $\vec{k}$ and polarization $\vec{\epsilon}$ span a plane which is referred to as the beam polarization plane. This plane is tilted by the angle φ with respect to the reaction plane which is defined by the final state momenta. Naturally, this plane builds the angle ϕ in the laboratory system. At the same time the angle of the beam polarization plane in the same reference frame is defined as α. It holds

$$\varphi = \alpha - \phi. \tag{4.2}$$

Figure 4.1 illustrates definitions of all angles and planes. Theoretically the beam asymmetry can be

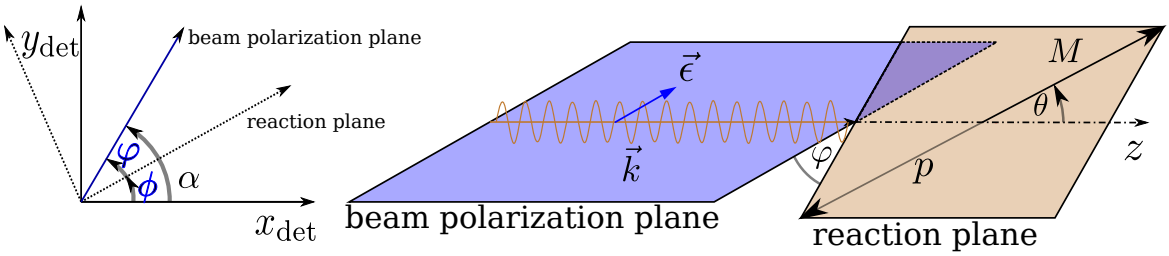

Figure 4.1: Left: Definition of angles α, ϕ, φ. Right: Photon momentum $\vec{k}$ and polarization $\vec{\epsilon}$ define the beam polarization plane while the reaction plane is defined by the recoil proton p and produced meson M.

determined by a measurement of the cross section and a fit using equation (4.1). However, when calculating polarized cross sections, it is important to have good control over flux normalization and detector acceptance in three dimensions $(E_\gamma, \cos\theta, \phi)$. To avoid this, the measurement of asymmetries

can be used to access the polarization observable Σ instead. Particularly, data is taken for two distinct orthogonal polarization settings corresponding to $\alpha = \pm 45^\circ$.

This chapter will illustrate the process of determining the beam asymmetry for η and η' photoproduction. The published results of Σ_η [Afz19; Afz+20] are used to check the accuracy and functionality of employed bayesian methods. Bayesian methods, as well as traditional frequentist approaches are used afterwards to extract new results for $\Sigma_{\eta'}$. First, the used methods will be presented and subsequently their application for each final state, respectively.

4.1 Methods

The beam asymmetry has to be determined via fits to ϕ distributions obtained from data. These are performed as either binned or unbinned fits. Both methods allow the application of Bayesian methods as will be discussed in the following. Additionally the advantages and disadvantages off all methods are compared.

4.1.1 Event yield asymmetries

Measurements were made in two distinct polarization settings $\alpha = \pm 45^\circ = \alpha^{\perp/\parallel}$. Thus, the polarized cross sections for both settings are given by[1]

$$\frac{\mathrm{d}\sigma^{\parallel}}{\mathrm{d}\Omega_{\mathrm{pol}}} = \frac{\mathrm{d}\sigma}{\mathrm{d}\Omega_0} \cdot \left[1 - p_\gamma^{\parallel} \Sigma \cos\left(2\left(\alpha^{\parallel} - \phi\right)\right)\right] \tag{4.3}$$

and

$$\frac{\mathrm{d}\sigma^{\perp}}{\mathrm{d}\Omega_{\mathrm{pol}}} = \frac{\mathrm{d}\sigma}{\mathrm{d}\Omega_0} \cdot \left[1 - p_\gamma^{\perp} \Sigma \cos\left(2\left(\alpha^{\perp} - \phi\right)\right)\right] \tag{4.4}$$

$$= \frac{\mathrm{d}\sigma}{\mathrm{d}\Omega_0} \cdot \left[1 + p_\gamma^{\perp} \Sigma \cos\left(2\left(\alpha^{\parallel} - \phi\right)\right)\right]. \tag{4.5}$$

Note that equation (4.5) holds, because

$$\alpha^{\perp} = \alpha^{\parallel} + \pi/2 \qquad \text{and} \qquad \cos x = -1 \cdot \cos(x + \pi).$$

Consider now taking the difference of equations (4.3) and (4.5)

$$\frac{\mathrm{d}\sigma^{\perp}}{\mathrm{d}\Omega_{\mathrm{pol}}} - \frac{\mathrm{d}\sigma^{\parallel}}{\mathrm{d}\Omega_{\mathrm{pol}}} = \frac{\mathrm{d}\sigma}{\mathrm{d}\Omega_0} \cdot \left(p_\gamma^{\perp} + p_\gamma^{\parallel}\right) \Sigma \cos\left(2\left(\alpha^{\parallel} - \phi\right)\right). \tag{4.6}$$

One can further eliminate the unpolarized cross section from this equation by dividing by the polarization weighted sum of equations (4.3) and (4.5)

$$\alpha \cdot \frac{\mathrm{d}\sigma^{\parallel}}{\mathrm{d}\Omega_{\mathrm{pol}}} + \beta \cdot \frac{\mathrm{d}\sigma^{\perp}}{\mathrm{d}\Omega_{\mathrm{pol}}} = \frac{\mathrm{d}\sigma}{\mathrm{d}\Omega_0} \cdot \left[\alpha + \beta - \left(\alpha p_\gamma^{\parallel} - \beta p_\gamma^{\perp}\right) \Sigma \cos\left(2\left(\alpha^{\perp} - \phi\right)\right)\right] \overset{!}{=} 2\frac{\mathrm{d}\sigma}{\mathrm{d}\Omega_0}. \tag{4.7}$$

[1] The dependencies of polarized and unpolarized cross sections as well as the beam asymmetry like in equation (4.1) are implied

Since

$$\frac{\mathrm{d}}{\mathrm{d}\phi}\frac{\mathrm{d}\sigma}{\mathrm{d}\Omega}_0 \stackrel{!}{=} 0 \forall \phi,$$

it holds

$$\alpha p_\gamma^{\parallel} - \beta p_\gamma^{\perp} \stackrel{!}{=} 0 \qquad\qquad \alpha + \beta \stackrel{!}{=} 2, \tag{4.8}$$

such that

$$\alpha = \frac{2p_\gamma^{\parallel}}{p_\gamma^{\perp} + p_\gamma^{\parallel}} \qquad\qquad \beta = \frac{2p_\gamma^{\perp}}{p_\gamma^{\perp} + p_\gamma^{\parallel}}. \tag{4.9}$$

The beam asymmetry Σ is thus accessible via the asymmetry

$$A(\phi) = \frac{\frac{\mathrm{d}\sigma}{\mathrm{d}\Omega}^{\perp}_{\mathrm{pol}} - \frac{\mathrm{d}\sigma}{\mathrm{d}\Omega}^{\parallel}_{\mathrm{pol}}}{p_\gamma^{\parallel}\frac{\mathrm{d}\sigma}{\mathrm{d}\Omega}^{\perp}_{\mathrm{pol}} + p_\gamma^{\perp}\frac{\mathrm{d}\sigma}{\mathrm{d}\Omega}^{\parallel}_{\mathrm{pol}}} = \Sigma \cos\left(2\left(\alpha^{\parallel} - \phi\right)\right). \tag{4.10}$$

At this point one can now make use of the fact that in any scattering reaction the number of events N is given by the product of luminosity L and total cross section σ

$$N = L \cdot \sigma = \Phi \cdot N_t \cdot \frac{\mathrm{d}\sigma}{\mathrm{d}\Omega} \cdot \Delta\Omega,$$

where Φ is the beam flux, N_t the number of target particles and $\Delta\Omega$ is the solid angle covered by the detector. Substituting this in equation (4.10) one can build the asymmetry $A(\phi)$ using only the (flux-)normalized event yields $\tilde{N}^{\parallel/\perp}\left(E_\gamma, \cos\theta, \phi\right)$[2]

$$A(\phi) = \frac{\tilde{N}^{\perp} - \tilde{N}^{\parallel}}{p_\gamma^{\parallel}\tilde{N}^{\perp} + p_\gamma^{\perp}\tilde{N}^{\parallel}} = \Sigma \cos\left(2\left(\alpha^{\parallel} - \phi\right)\right). \tag{4.11}$$

Alternatively, the event yields N can also be normalized by integrating over the total azimuthal angle range in each bin of $(E_\gamma, \cos\theta)$. This normalization technique has been used in reference [Afz19] and will also be used in this work. Using appropriate binning in ϕ in addition to beam energy and meson polar angle the asymmetry can be build for all kinematic bins and the beam asymmetry then be extracted via a one-Parameter fit. The statistical errors for $A(\phi)$ are given by Gaussian error propagation (see appendix A.1).

Frequentist

The beam asymmetry can now be determined via a frequentist fit, where Σ is determined such that the χ^2 value resulting from the data points and equation 4.11 is minimized. The results are point estimates with statistical error bars that are also obtained from the fit: $\hat{\Sigma} \pm \sigma_{\hat{\Sigma}}$. In addition $\chi^2/\mathrm{NDF} \approx 1$ may be verified in order to diagnose the fit itself. Multiple automated minimization and calculation

[2] again, arguments $\left(E_\gamma, \cos\theta, \phi\right)$ are implied.

algorithms for χ^2 fitting are available as open source. The *Python* [RP22] module *scipy* [Vir+20] and *ROOT* [BR97] offer e.g. the methods `scipy.optimize.curve_fit` [sci] and `TH1::Fit()` [ROO] for discrete/binned data, which were used in the analysis.

Bayesian

Following section 1.3, where the basics of Bayesian inference were discussed, the goal of a Bayesian approach is to sample marginal posterior distributions for each fitted parameter from the joint posterior $p(\boldsymbol{\theta}|y)$ which depends on the observed data y. The joint posterior itself is proportional to the product of priors $\pi(\boldsymbol{\theta})$ and likelihood $\mathcal{L}(y|\boldsymbol{\theta})$ (Bayes' theorem). This collapses to a one parameter problem in the case of fitting the event yield asymmetries (Eq. (4.11))

$$p(\Sigma|y) \propto \pi(\Sigma) \cdot \mathcal{L}(y|\Sigma). \tag{4.12}$$

However, to be able to sample from a joint posterior, prior and likelihood need to be specified. In order not to bias the fit towards any particular values, the prior is chosen non-informative, realized by a broad Gaussian centered at 0 which is truncated to the physically allowed parameter space of $\Sigma \in [-1, 1]$. Furthermore, the likelihood is formulated assuming Gaussian errors ϵ_n at each data point y_n, which should be described by the asymmetry (Eq (4.11)) at bin n $A(\phi_n; \Sigma)$, i. e. [3]

$$\Sigma \sim \mathcal{N}(0,1)_{[-1,1]} \qquad y_n = A\left(\phi_n; \Sigma\right) + \epsilon_n \qquad \epsilon_n \sim \mathcal{N}\left(0, \sigma_n\right), \tag{4.13}$$

which is equivalent to

$$\Sigma \sim \mathcal{N}(0,1) \qquad y_n \sim \mathcal{N}\left(A(\phi_n; \Sigma), \sigma_n\right). \tag{4.14}$$

The likelihood of all data points now evaluates to the product of the likelihood at each data point y_n and the posterior results in

$$p(\Sigma|y) \propto \pi(\Sigma) \cdot \mathcal{L}(y|\Sigma) = \mathcal{N}(\Sigma|0,1)_{[-1,1]} \cdot \prod_n \mathcal{N}\left(y_n | A\left(\phi_n; \Sigma\right), \sigma_n\right) \tag{4.15}$$

$$\Leftrightarrow -\ln p(\Sigma|y) = \frac{1}{2}\Sigma^2 + \frac{1}{2}\sum_n \left(\frac{y_n - A\left(\phi_n; \Sigma\right)}{\sigma_n}\right)^2 + \text{ constant terms}, \tag{4.16}$$

such that all ingredients are present to form a fully Bayesian probabilistic model[4]. This model was implemented in Stan [Sta22], directly giving access to samples from the posterior obtained with the No-U-Turn-Sampler (NUTS) [Sta22; HG14]. Hereby, the sampling is restricted to the allowed parameter region $\Sigma \in [-1, 1]$. As a measure of goodness of fit, the p-values obtained from the posterior predictive distributions, as introduced in section 1.3, are reviewed. To diagnose the convergence of the MCMC fit, sensible values for $\hat{R}$ and the Monte-Carlo standard error σ_{MCSE} are verified.

[3] Remember the notation introduced in section 1.3: $x \sim \mathcal{N}(\mu, \sigma) = \mathcal{N}(x|\mu, \sigma) = \frac{1}{\sqrt{2\pi\sigma^2}} e^{-\frac{(x-\mu)^2}{2\sigma^2}}$

[4] Note that the sampling aims only to reflect the right proportionality of the (marginal) posterior. Thus, constant terms can be dropped and are of no further interest [Sta22].

4.1.2 Event based fit

Although intuitive and easily implementable the binned fit –Bayesian or not– has one critical disadvantage: it is inevitable that information is lost because the asymmetry $A(\phi)$ is a binned quantity and hence, the choice of binning influences the fit results. This will be discussed in more detail in section 4.1.3. Especially kinematic bins with low statistics show this behavior. To circumvent this problem, an *unbinned fit*, based on the likelihood function for each event, can be performed. Also, no assumptions on the distribution of statistical errors have to be made since each event is taken into account individually. Yet, the event based fit does not provide any measure of goodness of fit, so that the study of toy Monte Carlo has to confirm the correct working principle of the method.

In a polarized experiment the azimuthal angle distribution of events is not isotropic, but modulated by a cosine term coupling to beam asymmetry Σ and beam polarization $p_\gamma^{\parallel/\perp}$ for each setting $\alpha^{\parallel/\perp}$, as is expressed through the respective differential cross sections in Equations 4.3 and 4.4. Since the number of events is proportional to the cross section, the probability $p(\phi|\Sigma)$ to find an event under the azimuthal angle ϕ for a given bin of $\left(E_\gamma, \cos\theta\right)$ is

$$p(\phi|\Sigma) \propto \left[1 \mp p_\gamma^{\parallel/\perp}\Sigma\cos\left(2\left(\alpha^\parallel - \phi\right)\right)\right]. \tag{4.17}$$

This is only true for an idealized experiment with acceptance $\epsilon = \text{const}\forall\phi$, so that the acceptance $\epsilon(\phi)$ has to be included in the probability for each event. As demonstrated in reference [Har17] a Fourier series truncated at 4 is sufficient to describe any occurring function

$$\epsilon(\phi) = \sum_{k=0}^{4} a_k \sin\left(k\phi\right) + b_k \cos\left(k\phi\right) \tag{4.18}$$

Frequentist

Bayesian

4.1.3 Comparison of Bayesian and frequentist approaches

4.2 Determination of Σ_η using Bayesian statistics

4.2.1 Event yield asymmetries

Application of method to toy Monte Carlo data

Application of method to data

4.2.2 Event based fit

Application of method to toy Monte Carlo data

Application of method to data

4.2.3 Discussion

4.3 Determination of $\Sigma_{\eta'}$

4.3.1 Application of event based fit to toy Monte Carlo data

4.3.2 Application of event based fit to data

4.3.3 Systematic Error

Bibliography

[Zyl+20] P. Zyla et al., *Review of Particle Physics*, PTEP **2020** (2020) 083C01.

[LMP01] U. Löring, B. Metsch and H. Petry, *The light-baryon spectrum in a relativistic quark model with instanton-induced quark forces*,
The European Physical Journal A **10** (2001) 395, ISSN: 1434-601X,
URL: http://dx.doi.org/10.1007/s100500170105.

[KS03] B. Krusche and S. Schadmand,
Study of nonstrange baryon resonances with meson photoproduction,
Prog. Part. Nucl. Phys. **51** (2003) 399, arXiv: nucl-ex/0306023.

[Afz19] F. N. Afzal, *Measurement of the beam and helicity asymmetries in the reactions $\gamma p \to p\pi^0$ and $\gamma p \to p\eta$*,
PhD thesis: Rheinische Friedrich-Wilhelms-Universität Bonn, 2019,
URL: https://hdl.handle.net/20.500.11811/8064 (cit. on pp. 4, 34, 35).

[DT92] D. Drechsel and L. Tiator, *Threshold pion photoproduction on nucleons*,
J. Phys. G **18** (1992) 449.

[Bar+18] M. Bartelmann et al., *Theoretische Physik 3 — Quantenmechanik*, 2018,
ISBN: 978-3-662-56071-6.

[Bar89] R. J. Barlow, *Statistics, A Guide to the Use of Statistical Methods in the Physical Sciences*,
Wiley, 1989.

[San+11] A. M. Sandorfi, S. Hoblit, H. Kamano and T.-S. H. Lee,
Determining pseudoscalar meson photoproduction amplitudes from complete experiments,
Journal of Physics G: Nuclear and Particle Physics **38** (2011) 053001, ISSN: 1361-6471,
URL: http://dx.doi.org/10.1088/0954-3899/38/5/053001 (cit. on p. 33).

[Afz+20] F. Afzal et al.,
Observation of the $p\eta'$ Cusp in the New Precise Beam Asymmetry Σ Data for $\gamma p \to p\eta$,
Phys. Rev. Lett. **125** (15 2020) 152002,
URL: https://link.aps.org/doi/10.1103/PhysRevLett.125.152002
(cit. on p. 34).

[RP22] G. van Rossum and the Python development team,
The Python Language Reference, Release 3.10.5, 2022,
URL: https://docs.python.org/3.10/reference/index.html (cit. on p. 36).

[Vir+20] P. Virtanen et al., *SciPy 1.0: Fundamental Algorithms for Scientific Computing in Python*,
Nature Methods **17** (2020) 261 (cit. on p. 36).

[BR97] R. Brun and F. Rademakers, *ROOT — An object oriented data analysis framework*, Nucl. Instrum. Meth. A **389** (1997) 81, ISSN: 0168-9002, URL: https://www.sciencedirect.com/science/article/pii/S016890029700048X (cit. on p. 36).

[sci] scipy, *scipy.optimize.curve_fit, Function Documentation*, URL: https://docs.scipy.org/doc/scipy/reference/generated/scipy.optimize.curve_fit.html (visited on 28/06/2022) (cit. on p. 36).

[ROO] ROOT, *TH1 Class reference*, URL: https://root.cern.ch/doc/master/classTH1.html#a63eb028df86bc86c8e20c989eb23fb2a (visited on 28/06/2022) (cit. on p. 36).

[Sta22] Stan development team, *Stan Modeling Language Users Guide and Reference Manual*, vol. 2.29, 2022, URL: https://mc-stan.org (cit. on p. 36).

[HG14] M. D. Hoffman and A. Gelman, *The No-U-Turn Sampler: Adaptively Setting Path Lengths in Hamiltonian Monte Carlo*, Journal of Machine Learning Research **15** (2014) 1593, URL: http://jmlr.org/papers/v15/hoffman14a.html (cit. on p. 36).

[Har17] J. Hartmann, *Measurement of Double Polarization Observables in the Reactions $\gamma p \to p\pi^0$ and $\gamma p \to p\eta$ with the Crystal Barrel/TAPS Experiment at ELSA*, Rheinische Friedrich-Wilhelms-Universität Bonn, 2017, URL: https://hdl.handle.net/20.500.11811/7258.

List of Figures

List of Tables